haematologica
Journal of the Ferrata Storti Foundation

Allograft inflammatory factor -1 is essential for acute monocytic leukemia infiltration

by Ai-Li Chen, Hai-Yang Hu, Doaa Alamoudi, Jia-Yang Zhang, Shi-Jie Yao, Bi-Huan Zhao, He-Yu Song, Hong-Hu Zhu and Qian-Fei Wang

Received: October 11, 2025.
Accepted: April 17, 2026.

Citation: Ai-Li Chen, Hai-Yang Hu, Doaa Alamoudi, Jia-Yang Zhang, Shi-Jie Yao, Bi-Huan Zhao, He-Yu Song, Hong-Hu Zhu and Qian-Fei Wang. Allograft inflammatory factor -1 is essential for acute monocytic leukemia infiltration.
Haematologica. 2026 Apr 23. doi: 10.3324/haematol.2025.300027 [Epub ahead of print]

Allograft inflammatory factor -1 is essential for acute monocytic leukemia infiltration

Ai-Li Chen[1, 2, 3, 4, *, #] Hai-Yang Hu[2, 3, 4, *, &], Doaa Alamoudi[2, 3, 4, &], Jia-Yang Zhang[5, 6], Shi-Jie Yao[2, 3, 4, &], Bi-Huan Zhao[7], He-Yu Song[7], Hong-Hu Zhu[5, 7], Qian-Fei Wang[2, 3, 4, #]

[1] *Medical Research Center, Beijing Chao-Yang Hospital, Capital Medical University, Beijing 100020, China*

[2] *China National Center for Bioinformation, Beijing 10010l, China*

[3] *Beijing Institute of Genomics, Chinese Academy of Sciences, Beijing 100101, China*

[4] *University of Chinese Academy of Sciences, Beijing 100049, China*

[5] *Department of Hematology, Beijing Chao-Yang Hospital, Capital Medical University, Beijing 100020, China*

[6]*The Postgraduate Training Base of Jinzhou Medical University (The PLA Rocket Force Characteristic Medical Center), Beijing 100032, China*

[7] *Chinese Institute for Medical Research, Capital Medical University, Beijing 100069, China*

[&]***Current address:***

Hai-Yang Hu: Beijing An Zhen Hospital, Capital Medical University, Beijing 100029, China; Beijing Institute of Heart, Lung and Blood Vessel Diseases, Beijing 100029, China

Doaa Alamoudi: Genomic Medicine Center of Excellence, King Faisal Specialist Hospital & Research Centre, Riyadh, Saudi Arabia.

Shi-Jie Yao: Department of Cell Biology, School of Basic Medical Sciences, Peking University Health Science Center, Peking University, Beijing 100191, China

[*] CAL and HHY contributed equally as co-first authors.

[#] Correspondence:

E-mail: chenal@mail.ccmu.edu.cn (CAL); wangqf@big.ac.cn (WQF).

Running heads: AIF1 promotes monocytic leukemia infiltration

Acknowledgments
We thank Dr. Gang Huang (at University of Texas Health San Antonio) and Dr. Shaoyan Hu (at Children's Hospital of Soochow University) for their scientific and technical support.

Funding
This research was supported by the Beijing Natural Science Foundation (L234037 to CAL), the National Natural Science Foundation of China (82570206, 81970174 to CAL), the Fundamental and Interdisciplinary Disciplines Breakthrough Plan of the Ministry of Education of China (JYB2025XDXM612 to WQF) and The Beijing High-Level Innovation and Entrepreneurship Talent Support Program-young backbone talent projects (G202532253 to CAL).

Author Contributions
Ai-Li Chen: Conceptualization, Funding acquisition, Investigation, Methodology, Project administration, Supervision, Validation, Visualization, Writing – original draft, Writing – review & editing. **Hai-Yang Hu:** Data curation, Formal analysis, Visualization, Writing – original draft, Writing – review & editing. **Doaa Alamoudi:** Investigation, Validation**. Jia-Yang Zhang:** Investigation, Validation**. Shi-Jie Yao:** Investigation, Validation**. Bi-Huan Zhao:** Investigation, Validation**. He-Yu Song:** Investigation, Validation**. Hong-Hu Zhu:** Resources, Writing – review & editing. **Qian-Fei Wang:** Conceptualization, Project administration, Resources, Supervision, Writing – review & editing. All authors have read and approved the final manuscript.

Competing Interests
The authors declare no competing financial interests.

Data-sharing statement
The bulk RNA-sequencing data generated in this study are deposited in the Genome Sequence Archive (GSA) under accession code HRA005186. The public datasets used in this study are available from The Cancer Genome Atlas (TCGA), the Therapeutically Applicable Research to Generate Effective Treatments (TARGET),

the Beat AML cohort, and the Gene Expression Omnibus (GEO) under accession codes GSE1159, GSE6891, GSE12417, GSE14468, and GSE37642.

To the editor:

Extramedullary infiltration (EMI) occurs in 2–9% of newly diagnosed acute myeloid leukemia (AML) patients[1] and is a high-risk feature associated with relapse[2,3]. EMI involves tissues not typically involved in hematopoiesis, including skin, central nervous system, and gingivae, complicating diagnosis, prognosis, and treatment. Extensive investigation has found no clear association with intramedullary cytogenetics. However, EMI cases frequently show monoblastic/myelomonocytic differentiation (43–81% of cases)[4] and a higher prevalence of the FAB M5 subtype[2,3], suggesting that distinct biological features of acute monoblastic/monocytic leukemia (AMoL) may underlie its tissue infiltration propensity. Here we reveal that infiltration-associated pathways are a distinct biological feature in AMoL, and identify AIF1 as a critical regulator of AMoL infiltration via the CCR2-MAPK axis.

To investigate whether infiltration-associated pathways represent a distinct biological feature of AMoL and to elucidate the underlying mechanisms driving the frequent occurrence of EMI, we conducted a comparative analysis of the expression profiles between AMoL and other AML subtypes across four public AML cohorts (TARGET, TCGA, GSE1159, and GSE6891). In line with the clinical phenotype, we identified specific enrichment of infiltration-associated characteristics related to cellular adhesion and migration in AMoL subtypes (Supplementary Figure S1A). We further identified eight infiltration-associated genes that are both relatively highly expressed in hematopoietic system and consistently upregulated in AMoL compared to other AML subtypes across all four cohorts (Supplementary Figure S1B). Among these eight tightly interconnected genes, allograft inflammatory factor-1 (*AIF1*) emerges as the most highly connected hub, with computational predictions suggesting functional linkages to six others (Supplementary Figure S1C). *AIF1* has been reported to be associated with tumor growth and migration in breast cancer[5,6] and renal cell carcinoma[7]. However, its functional role in AML remains poorly defined.

To clarify the potential involvement of *AIF1* in AMoL, we performed a comprehensive analysis of *AIF1* using public datasets, complemented by experimental validation. We found that *AIF1* expression was specifically elevated in AMoL (FAB-M5) and acute myelomonocytic leukemia (AMML, FAB-M4), compared with other AML subtypes and healthy controls (Figure 1A/B, Supplementary Figure S1D-F). Furthermore, AML samples with monocytic differentiation, as defined by CD14 expression via flow cytometry, exhibited significantly higher *AIF1* levels relative to both primitive AML and healthy $CD14^+$ monocytes (Figure 1B, Supplementary Figure S1D/E). To assess whether *AIF1* expression was restricted to monocytic blasts, we analyzed single-cell RNA sequencing data from pediatric AMoL and AMML bone marrow samples[8], revealing that *AIF1* expression was predominantly enriched in granulocyte/monocyte-like leukemic subpopulations (Supplementary Figure S1G). We

first confirmed that AIF1 expression was significantly enriched at both the transcriptional and protein levels in M5 and a subset of M4 leukemia cell lines compared to other subtypes (Figure 1C). To investigate the functional role of *AIF1* in AMoL, we performed knockdown (KD) using lentiviral shRNAs followed by reconstitution in the AMoL cell line THP-1. Both shRNAs effectively reduced AIF1 expression at the transcriptional and protein levels (Figure 1D) and significantly inhibited AMoL cell proliferation *in vitro*. Notably, this proliferative defect was partially rescued by AIF1 re-expression (Figure 1E). This anti-proliferative effect of *AIF1* KD was consistently observed in additional AML cell lines with monocytic features, including U937, MV4-11, and OCI-AML3 (Supplementary Figure S2A), but had minimal impact on non-monocytic AML cells (Kasumi-1 and K562) (Supplementary Figure S2B). Mechanistically, *AIF1* KD reduced self-renewal capacity and induced apoptosis, with minimal impact on cell cycle (Figure 1F, Supplementary Figure S2C).

To further explore whether *AIF1* contributes to AMoL EMI, transwell assays and adhesion assay were performed. *AIF1* KD remarkably reduced migration and infiltration capacities in both MLL-rearranged (THP-1) and non-rearranged (U937) cells, and this phenotype could be rescued by *AIF1* re-expression (Figure 2A/B, Supplementary Figure S2D). Conversely, overexpression of *AIF1* in Kasumi-1 cells—an M2 line with low endogenous AIF1 expression—significantly enhanced their migratory capacity (Supplementary Figure S2E). *AIF1* depletion also reduced adhesion to MS-5 stromal cells (Supplementary Figure S2F). *In vivo*, following the transplantation of THP-1 cells into NSG mice [which has been reviewed and approved by the Ethics Committee of the Beijing Institute of Genomics, Chinese Academy of Sciences (China National Center for Bioinformation) (Approval No. 2023A018) and the Institutional Animal Care and Use Committee (IACUC) of Beijing Chaoyang Hospital, Capital Medical University (Approval No. 25-2150)], we detected varying degrees of leukemic infiltration in multiple organs, including the liver, spleen, kidneys, and even the brain. Notably, *AIF1* KD consistently attenuated this infiltration across all examined organs, with the most significant suppression observed in the liver (Figure 2C, Supplementary Figure S2G).

Moreover, high *AIF1* levels significantly correlated with inferior event-free survival (EFS) and overall survival (OS) in both pediatric (TARGET) and adult (TCGA) AML cohorts (Figure 2D, Supplementary Figure S1H), and were elevated in intermediate/high-risk patients (Supplementary Figure S1F). Notably, *AIF1* levels further stratified EFS and OS outcomes within both M4/M5 or M1/M2 FAB subtypes (Supplementary Figure S1I/J). Consistently, *AIF1* KD significantly delayed leukemia onset and prolonged survival in the THP-1-derived xenograft model (Figure 2E), reinforcing the role of *AIF1* as a potential adverse prognostic marker in AMoL.

To investigate the underlying mechanism of *AIF1* in AMoL development and infiltration, transcriptomic sequencing (RNA-seq) was performed to identify the potential downstream genes and pathways regulated by AIF1. After *AIF1* KD, downregulated genes were mainly enriched in cell adhesion, cell death, immune activation and kinase signaling pathways (Supplementary Figure S3A). To identify potential downstream effectors of AIF1, we focused on genes that were significantly upregulated in FAB-M4 and M5 AML subtypes and exhibited strong correlation with *AIF1* expression in both our RNA-seq data and public AML datasets. Among these, *CCR2* (C-C chemokine receptor type 2) exhibited the most pronounced downregulation upon *AIF1* KD in both THP-1 and U937 monocytic AML cell lines, as validated by flow cytometry and quantitative PCR (Supplementary Figure S3B-E). Notably, CCR2 resides within the subset of six genes predicted to exhibit functional interactions with AIF1 among the eight candidate genes identified previously (Supplementary Figure S1C). Moreover, the expression of *CCR2* was specifically and consistently highly expressed in M4 and M5 patients and showed a significant positive correlation with *AIF1* expression across multiple public cohorts (Supplementary Figure S3F/G). CCR2 is a member of the G protein-coupled receptor (GPCR) family and functions as a receptor for chemokines such as CCL2 (monocyte chemoattractant protein-1, MCP-1). Previous studies have demonstrated that the CCL2–CCR2 signaling axis promotes tumor progression and migration through activation of the MAPK pathway[9]. Consistently, *AIF1* KD in AML cell lines led to significant downregulation of MAPK pathway–related genes in our RNA-seq data (Figure 3A). Simultaneously, GSEA results also indicate that in public cohorts, AML patients with high *AIF1* expression, regardless of disease subtype, exhibited activation of the MAPK pathway (Figure 3B). Western blot showed a decreased CCR2 expression and phosphorylation of p38 MAPK after *AIF1* KD (Figure 3C), suggesting that CCR2-MAPK axis supports AIF1 mediated leukemia cell migration and infiltration.

To further validate whether CCR2-MAPK axis could serve as a potential target for inhibiting AMoL infiltration, we treated THP-1 cells with RS504393 (a CCR2 inhibitor) and Adezmapimod (a p38 MAPK inhibitor), and found both drugs could impair the migration capacity of AMoL cells *in vitro* (Figure 3D). Moreover, treatment with either RS504393 or Adezmapimod significantly reduced leukemic infiltration across multiple organs in THP-1-derived xenograft model, with the most pronounced suppression observed in the liver and kidneys (Figure 3E). Collectively, these findings indicate that the AIF1–CCR2–MAPK axis plays a pivotal role in mediating AMoL infiltration and that therapeutic targeting of CCR2, in particular, may offer a promising strategy for the treatment of AMoL.

In this study, we demonstrate for the first time that *AIF1* overexpression promotes leukemic infiltration in AMoL, with CCR2 identified as a downstream effector. *AIF1*

was originally discovered in rat cardiac allografts undergoing chronic rejection [10], and is expressed in microglia, macrophages, T cells, synoviocytes, and adipocytes during inflammatory processes, playing a pivotal role in immune regulation and inflammation-associated pathologies[11]. Aberrant *AIF1* upregulation has been implicated in inflammatory disorders, transplant rejection, autoimmune diseases, and various malignancies. While the CCL2/CCR2 axis is a well-recognized pathway for monocyte migration[12], its contribution in the context of monocytic leukemia cell trafficking has been understudied. Prior studies have primarily focused on the CXCR4–CXCL12 axis[13] and matrix metalloproteinase (MMP) family proteins[14], highlighting a gap in our understanding of CCR2-mediated mechanisms in leukemic infiltration. Our findings identify AIF1 as a regulator of CCR2 and the MAPK signaling pathway. Notably, *AIF1* impaired monocytic leukemia cell migration and infiltration both *in vitro* and *in vivo* in a dose-dependent manner, correlating with the degree of KD efficiency. While the use of a p38 MAPK activator would further substantiate the rescue of the *AIF1* KD phenotype, the precise molecular mechanisms by which AIF1 governs this regulation warrant further investigation. Moreover, AIF1 has also been reported to bind directly to F-actin and Rho family GTPases such as Rac, thereby promoting membrane ruffling and phagocytosis[15], whether this represents an alternative mechanism contributing to AMoL cell migration remains to be explored.

Our study also highlights the feasibility of targeting the CCR2 or MAPK pathways as potential therapeutic strategies for AMoL and EMI in AML. While previous studies suggest that EMI may facilitate disease relapse, its prognostic relevance in AML remains controversial[1,4]. In our analysis, *AIF1* was highly expressed in both AMML and AMoL (FAB M4 and M5), AMML frequently harbors the CBFβ–MYH11 fusion gene associated with favorable prognosis, which may partly explain the therapeutic dilemma in treating EMI cases. Our data further indicate that, in the context of AMoL, EMI may be associated with inferior clinical outcomes. Collectively, these findings provide novel insights into the pathogenesis of AMoL and repose new avenues for therapeutic intervention in EMI-associated AML.

Reference:

1. Solh M, Solomon S, Morris L, Holland K, Bashey A. Extramedullary acute myelogenous leukemia. Blood Rev. 2016;30(5):333-339.
2. Kobayashi R, Tawa A, Hanada R, Horibe K, Tsuchida M, Tsukimoto I. Extramedullary infiltration at diagnosis and prognosis in children with acute myelogenous leukemia. Pediatr Blood Cancer. 2007;48(4):393-398.
3. Hu GH, Lu AD, Jia YP, Zuo YX, Wu J, Zhang LP. Prognostic Impact of Extramedullary Infiltration in Pediatric Low-risk Acute Myeloid Leukemia: A Retrospective Single-center Study Over 10 Years. Clin Lymphoma Myeloma Leuk. 2020;20(11):e813-e820.
4. Shallis RM, Gale RP, Lazarus HM, et al. Myeloid sarcoma, chloroma, or extramedullary acute myeloid leukemia tumor: A tale of misnomers, controversy and the unresolved. Blood Rev. 2021;47:100773.
5. Li T, Feng Z, Jia S, et al. Daintain/AIF-1 promotes breast cancer cell migration by up-regulated TNF-α via activate p38 MAPK signaling pathway. Breast Cancer Res Treat. 2012;131(3):891-898.
6. Liu S, Tan WY, Chen QR, et al. Daintain/AIF-1 promotes breast cancer proliferation via activation of the NF-kappaB/cyclin D1 pathway and facilitates tumor growth. Cancer Sci. 2008;99(5):952-957.
7. Liu X, Zhang D, Hu J, Xu S, Xu C, Shen Y. Allograft inflammatory factor 1 is a potential diagnostic, immunological, and prognostic biomarker in pan-cancer. Aging (Albany NY). 2023;15(7):2582-2609.
8. Zhang Y, Jiang S, He F, et al. Single-cell transcriptomics reveals multiple chemoresistant properties in leukemic stem and progenitor cells in pediatric AML. Genome Biol. 2023;24(1):199.
9. Xu M, Wang Y, Xia R, Wei Y, Wei X. Role of the CCL2-CCR2 signalling axis in cancer: Mechanisms and therapeutic targeting. Cell Prolif. 2021;54(10):e13115.
10. Utans U, Arceci RJ, Yamashita Y, Russell ME. Cloning and characterization of allograft inflammatory factor-1: a novel macrophage factor identified in rat cardiac allografts with chronic rejection. J Clin Invest. 1995;95(6):2954-2962.
11. Sikora M, Kopeć B, Piotrowska K, Pawlik A. Role of allograft inflammatory factor-1 in pathogenesis of diseases. Immunol Lett. 2020;218:1-4.
12. Shi C, Pamer EG. Monocyte recruitment during infection and inflammation. Nat Rev Immunol. 2011;11(11):762-774.
13. Ladikou EE, Chevassut T, Pepper CJ, Pepper AG. Dissecting the role of the CXCL12/CXCR4 axis in acute myeloid leukaemia. Br J Haematol. 2020;189(5):815-825.

14. Paupert J, Mansat-De Mas V, Demur C, Salles B, Muller C. Cell-surface MMP-9 regulates the invasive capacity of leukemia blast cells with monocytic features. Cell Cycle. 2008;7(8):1047-1053.
15. De Leon-Oliva D, Garcia-Montero C, Fraile-Martinez O, et al. AIF1: function and connection with inflammatory diseases. Biology (Basel). 2023;12(5):694.

Figure Legends:

Figure 1. *AIF1* is highly expressed and plays an important role in AMoL.

A. Expression levels of *AIF1* across different FAB subtypes in the TCGA AML cohort. The dashed line represents the mean expression level of *AIF1* across all samples.

B. The expression of *AIF1* in different AML FAB subtypes, and *AIF1*/ACTB ratios in $CD14^+$ monocytes from healthy donors (N= 10) vs. M4, M5 (N=53, N=25) or CD14 top quartile AML patient blasts (N=60) in GSE12417.

C. AIF1 expression levels (transcriptional and protein) in various cell lines representing different subtypes and in healthy donors. GAPDH expression is used as a control. HD, healthy donor.

D. AIF1 expression levels (transcriptional and protein) in THP-1 cells transduced with scramble control (shCon), *AIF1* shRNAs (sh*AIF1*-1/2) and/or *AIF1* cDNA (+*AIF1*) by lentivirus. RNA was extracted 48 hours after cell sorting, and *AIF1* expression was quantified by real-time quantitative PCR. Relative *AIF1* expression of each sample was normalized to its GAPDH expression and then compared with shCon. Data come from a single experiment, representative of 3 independent experiments.

E. Growth curves of THP-1 cells were transduced with shCon, sh*AIF1* and/or *AIF1*. Cell number (y axis) and days (x axis) are indicated. Data come from a single experiment, representative of 3 independent experiments.

F. Colony-forming-unit (CFU) assay of THP-1 cells transduced with shCon or sh*AIF1*, cells were planted in MethoCult™ H4230 with 20% FBS, and the cell colonies were counted after 14 days. Data come from a single experiment, representative of 3 independent experiments.

Statistical significance: *p<0.05, **p<0.01, ***p<0.001.

Comparisons: * vs. shCon (t-test) or mean expression level of *AIF1* (Anova test)，# vs. +*AIF1*, $ vs. sh*AIF1*-1, & vs. sh*AIF1*-2 (t-test).

Figure 2. *AIF1* promotes the migration and infiltration of AMoL and impacts survival.

A. Transwell migration assay of THP-1 cells transduced with shCon, sh*AIF1* and/or *AIF1*. Cells were serum-starved for 20 hours, then seeded into the upper chamber. The lower chamber contained RPMI 1640 medium with 20% FBS. After 2 hours of incubation at 37°C with 5% CO_2, cells migrated to the lower chamber are counted to calculate migrate ratio. The images show cells that had migrated to the lower chamber, visualized under 10× magnification. Scale bar, 200um.

B. Migration rate of THP-1 cells transduced with shCon, sh*AIF1* and/or *AIF1,* calculated as the ratio of cells that migrated to the lower chamber to the total number of cells seeded in the upper chamber. All experiments included plating controls to

ensure equal seeding across groups. Quantification represents three biological replicates with three technical replicates each.

C. Liver infiltration of NSG mice receiving THP-1 cells transduced with shCon or sh*AIF1*, the infiltration ratio quantified as the ratio of THP-1 cell abundance in the liver relative to that in the bone marrow from the same mouse.

D. Kaplan-Meier curves showing the event-free survival (EFS) and overall survival (OS) of TCGA-AML patients, stratified by the median expression of *AIF1*.

E. Survival curves of NSGS mice receiving 250,000 sorted THP-1 cells transduced with shCon or sh*AIF1* (n=4). The overall p-value is shown in the figure (log-rank test). For sh*AIF1*-1 versus shCon: p=0.0067; for sh*AIF1*-2 versus shCon: p=0.3962.

Statistical significance: *p<0.05, **p<0.01, ***p<0.001.

Comparisons: * vs. shCon，# vs. +*AIF1*, $ vs. sh*AIF1*-1, & vs. sh*AIF1*-2 (t-test).

Figure 3. The AIF1—CCR2—MAPK axis is essential for AMoL infiltration.

A. Expression of partial genes involved in the MAPK pathway when knockdown using sh*AIF1*-1 or sh*AIF1*-2 or empty control in THP-1 and U937 cell lines.

B. Enhanced MAPK pathway activity in the top one-third of AML patients with higher AIF1 expression compared to the bottom one-third of patients with lower AIF1 expression in FAB M2 and M5 subtypes of the BeatAML cohort (GSEA).

C. Endogenous CCR2, phosphorated p38 MAPK and p38 MAPK expression of THP-1 cells (knockdown or rescue *AIF1*) were detected by western blot, GAPDH was used as loading control.

D. Transwell migration assay of THP-1 cells treated with RS504393 (CCR2i) or Adezmapimod (p38 MAPKi). Cells were treated with no serum RPMI 1640 medium for 2h, then treated with DMSO, RS504393 (25uM) and Adezmapimod (10uM), respectively, placed into the Transwell insert where the lower chamber contain RPMI 1640 medium with 20% serum, incubated at 37°C, 5% CO_2 for 2h, cells migrated to the lower chamber were counted to calculate migration ratios.

E. Liver and kidney infiltration ratio of NSG mice receiving THP-1 cells then treated with RS504393 or Adezmapimod. Both drugs were administered intraperitoneally at 5 mg/kg from the 10th day post-transplantation, every other day for 5 doses. The infiltration ratio quantified as the ratio of THP-1 cell abundance in the liver/kidney relative to that in the bone marrow from the same mouse.

Statistical significance: *p<0.05, **p<0.01, ***p<0.001

Comparisons: * vs. DMSO (t-test).

Figure_1

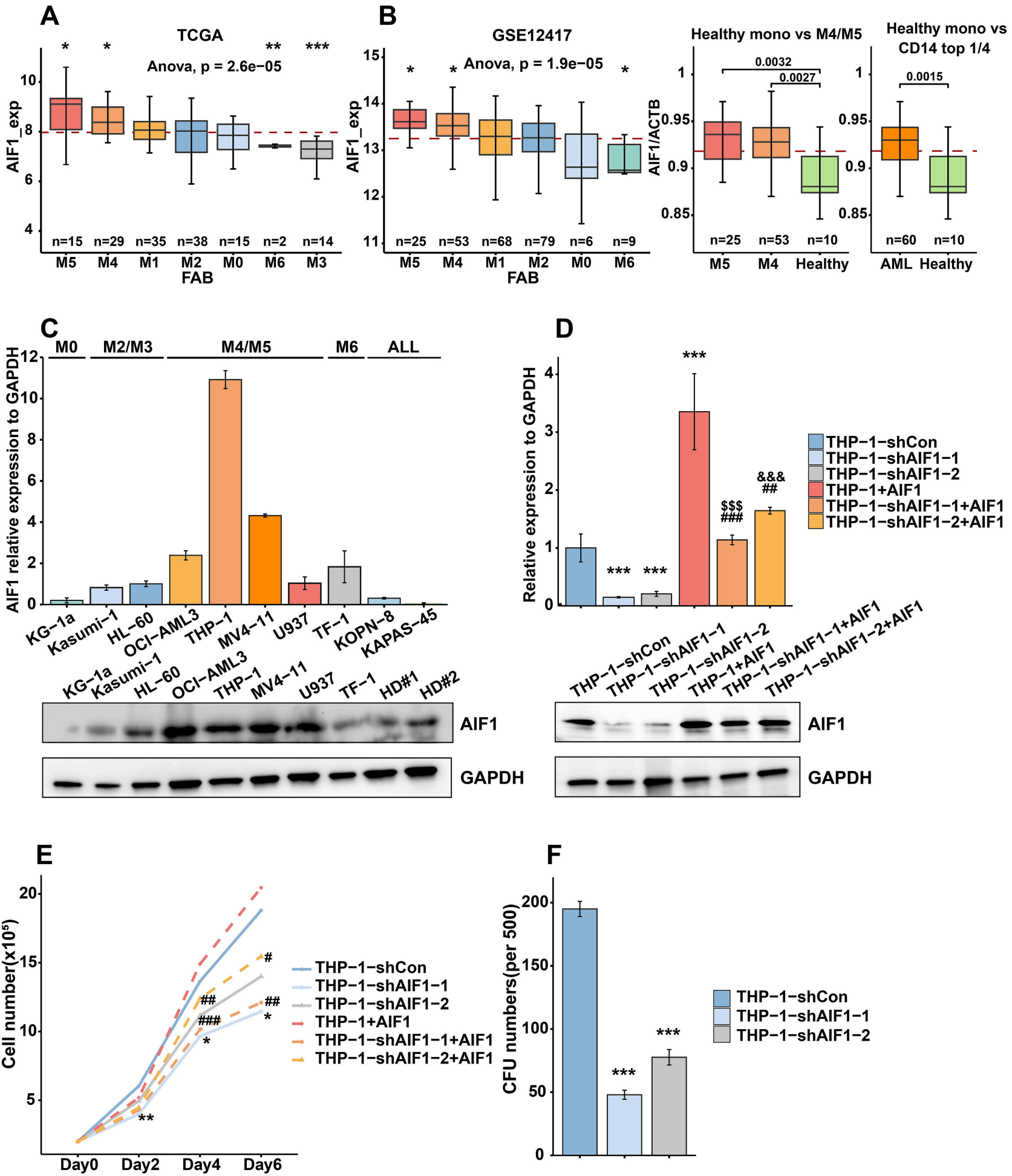
A
TCGA
Anova, p = 2.6e−05
AIF1_exp
n=15 n=29 n=35 n=38 n=15 n=2 n=14
M5 M4 M1 M2 M0 M6 M3
FAB
B
GSE12417
Anova, p = 1.9e−05
AIF1_exp
n=25 n=53 n=68 n=79 n=6 n=9
M5 M4 M1 M2 M0 M6
FAB
Healthy mono vs M4/M5
0.0032
0.0027
AIF1/ACTB
n=25 n=53 n=10
M5 M4 Healthy
Healthy mono vs CD14 top 1/4
0.0015
n=60 n=10
AML Healthy
C
M0 M2/M3 M4/M5 M6 ALL
AIF1 relative expression to GAPDH
KG−1a Kasumi−1 HL−60 OCI−AML3 THP−1 MV4−11 U937 TF−1 KOPN−8 KAPAS−45
KG−1a Kasumi−1 HL−60 OCI−AML3 THP−1 MV4−11 U937 TF−1 HD#1 HD#2
AIF1
GAPDH
D
Relative expression to GAPDH
THP−1−shCon
THP−1−shAIF1−1
THP−1−shAIF1−2
THP−1+AIF1
THP−1−shAIF1−1+AIF1
THP−1−shAIF1−2+AIF1
THP−1−shCon THP−1−shAIF1−1 THP−1−shAIF1−2 THP−1+AIF1 THP−1−shAIF1−1+AIF1 THP−1−shAIF1−2+AIF1
AIF1
GAPDH
E
Cell number(x10⁵)
Day0 Day2 Day4 Day6
THP−1−shCon
THP−1−shAIF1−1
THP−1−shAIF1−2
THP−1+AIF1
THP−1−shAIF1−1+AIF1
THP−1−shAIF1−2+AIF1
F
CFU numbers(per 500)
THP−1−shCon
THP−1−shAIF1−1
THP−1−shAIF1−2

Figure_2

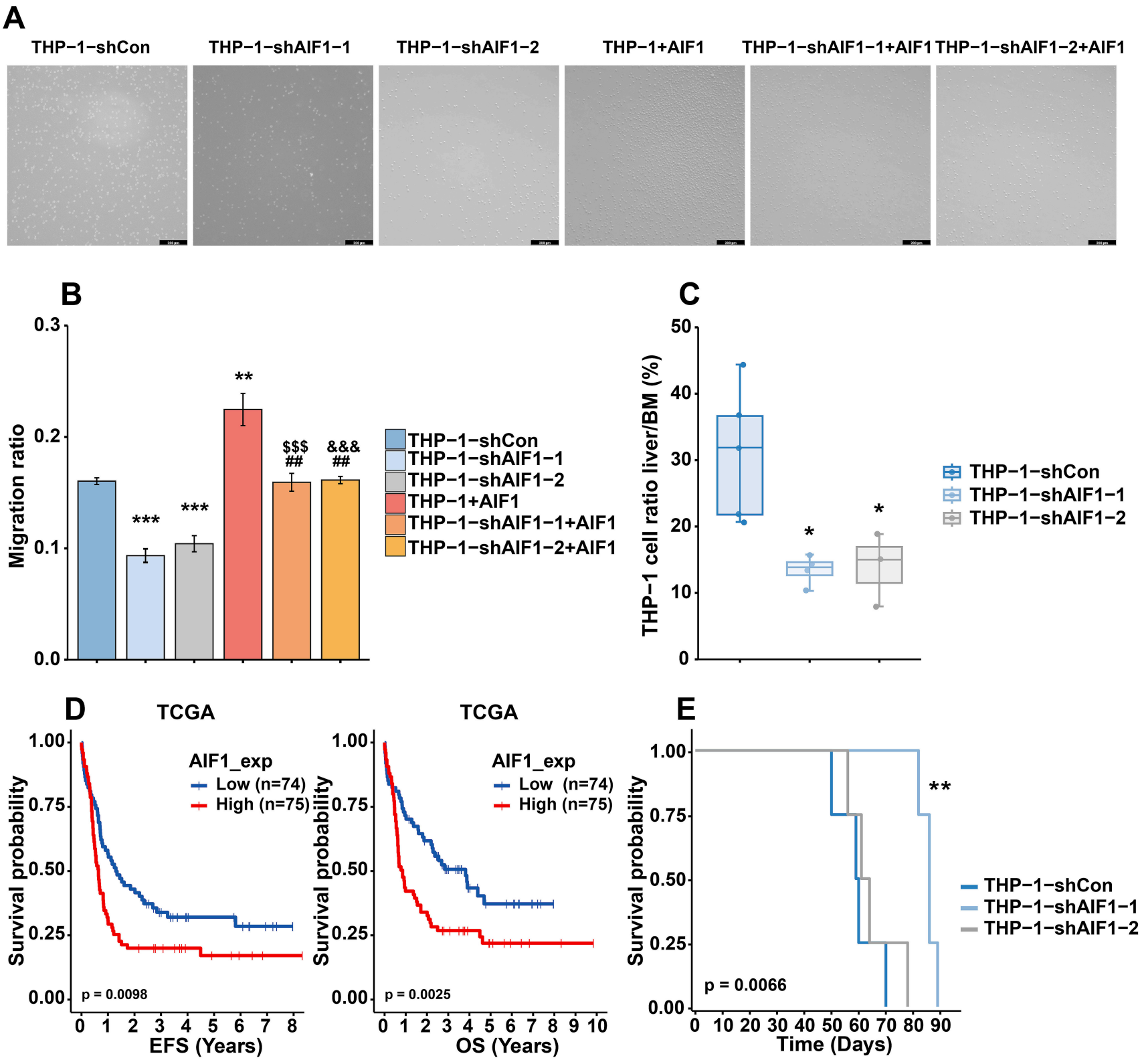
A
THP−1−shCon
THP−1−shAIF1−1
THP−1−shAIF1−2
THP−1+AIF1
THP−1−shAIF1−1+AIF1
THP−1−shAIF1−2+AIF1
B
Migration ratio
0.0
0.1
0.2
0.3
***
***
**
$$$
##
&&&
##
THP−1−shCon
THP−1−shAIF1−1
THP−1−shAIF1−2
THP−1+AIF1
THP−1−shAIF1−1+AIF1
THP−1−shAIF1−2+AIF1
C
THP−1 cell ratio liver/BM (%)
0
10
20
30
40
50
*
*
THP−1−shCon
THP−1−shAIF1−1
THP−1−shAIF1−2
D
TCGA
Survival probability
0.00
0.25
0.50
0.75
1.00
AIF1_exp
Low (n=74)
High (n=75)
p = 0.0098
0 1 2 3 4 5 6 7 8
EFS (Years)
TCGA
Survival probability
0.00
0.25
0.50
0.75
1.00
AIF1_exp
Low (n=74)
High (n=75)
p = 0.0025
0 1 2 3 4 5 6 7 8 9 10
OS (Years)
E
Survival probability
0.00
0.25
0.50
0.75
1.00
**
p = 0.0066
0 10 20 30 40 50 60 70 80 90
Time (Days)
THP−1−shCon
THP−1−shAIF1−1
THP−1−shAIF1−2

Figure_3

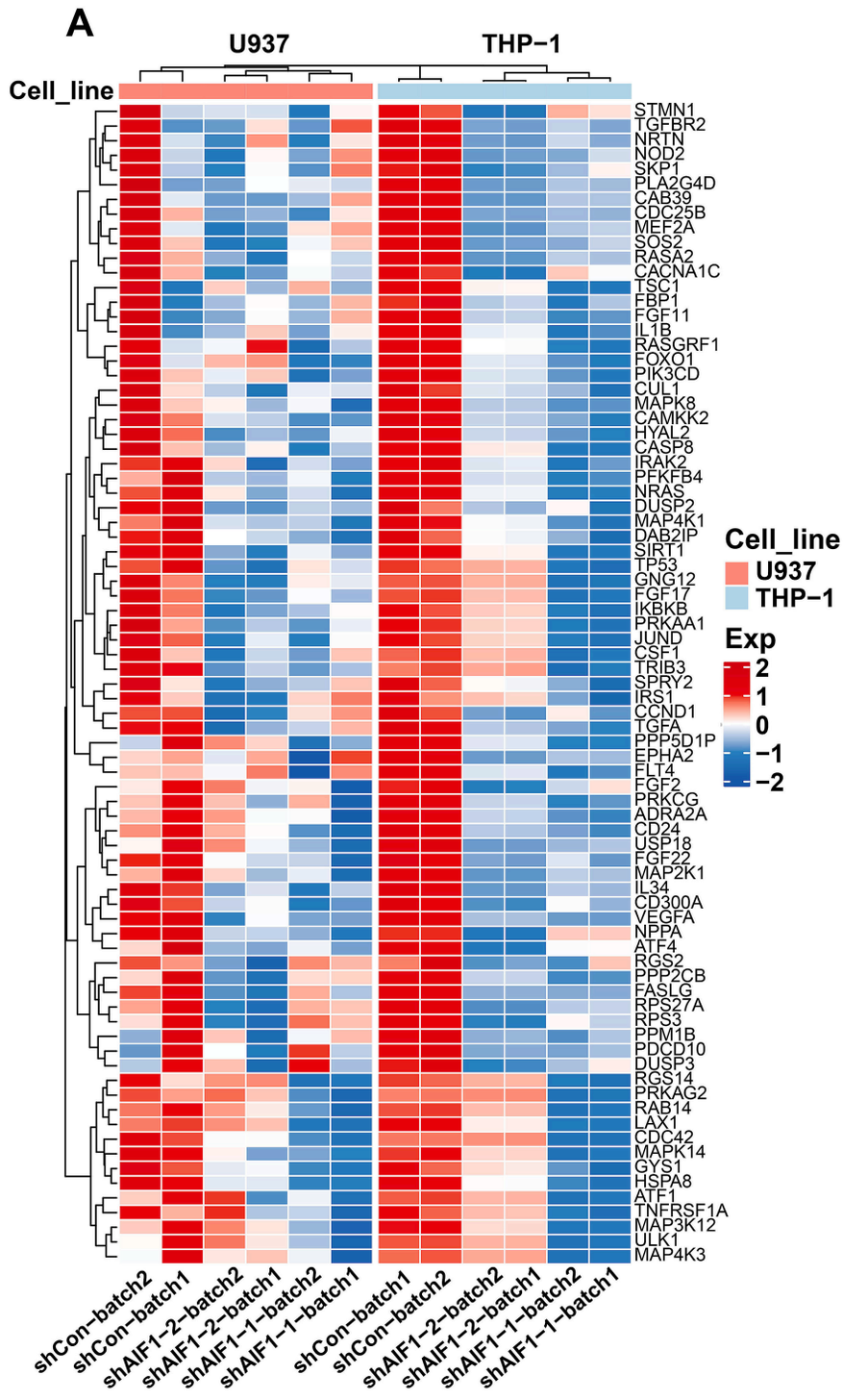
A
U937
THP−1
Cell_line
STMN1
TGFBR2
NRTN
NOD2
SKP1
PLA2G4D
CAB39
CDC25B
MEF2A
SOS2
RASA2
CACNA1C
TSC1
FBP1
FGF11
IL1B
RASGRF1
FOXO1
PIK3CD
CUL1
MAPK8
CAMKK2
HYAL2
CASP8
IRAK2
PFKFB4
NRAS
DUSP2
MAP4K1
DAB2IP
SIRT1
TP53
GNG12
FGF17
IKBKB
PRKAA1
JUND
CSF1
TRIB3
SPRY2
IRS1
CCND1
TGFA
PPP5D1P
EPHA2
FLT4
FGF2
PRKCG
ADRA2A
CD24
USP18
FGF22
MAP2K1
IL34
CD300A
VEGFA
NPPA
ATF4
RGS2
PPP2CB
FASLG
RPS27A
RPS3
PPM1B
PDCD10
DUSP3
RGS14
PRKAG2
RAB14
LAX1
CDC42
MAPK14
GYS1
HSPA8
ATF1
TNFRSF1A
MAP3K12
ULK1
MAP4K3
Cell_line
U937
THP−1
Exp
2
1
0
−1
−2
shCon−batch2
shCon−batch1
shAIF1−2−batch2
shAIF1−2−batch1
shAIF1−1−batch2
shAIF1−1−batch1
shCon−batch1
shCon−batch2
shAIF1−2−batch2
shAIF1−2−batch1
shAIF1−1−batch2
shAIF1−1−batch1

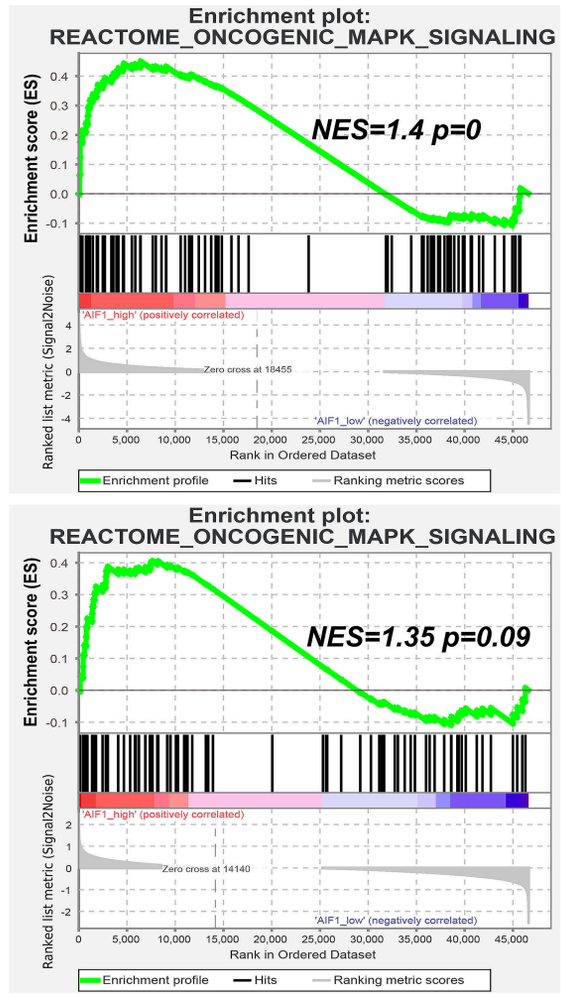
B
Enrichment plot:
REACTOME_ONCOGENIC_MAPK_SIGNALING
NES=1.4 p=0
Enrichment score (ES)
'AIF1_high' (positively correlated)
Zero cross at 16455
'AIF1_low' (negatively correlated)
Ranked list metric (Signal2Noise)
Rank in Ordered Dataset
Enrichment profile
Hits
Ranking metric scores
Enrichment plot:
REACTOME_ONCOGENIC_MAPK_SIGNALING
NES=1.35 p=0.09
Enrichment score (ES)
'AIF1_high' (positively correlated)
Zero cross at 14140
'AIF1_low' (negatively correlated)
Ranked list metric (Signal2Noise)
Rank in Ordered Dataset
Enrichment profile
Hits
Ranking metric scores

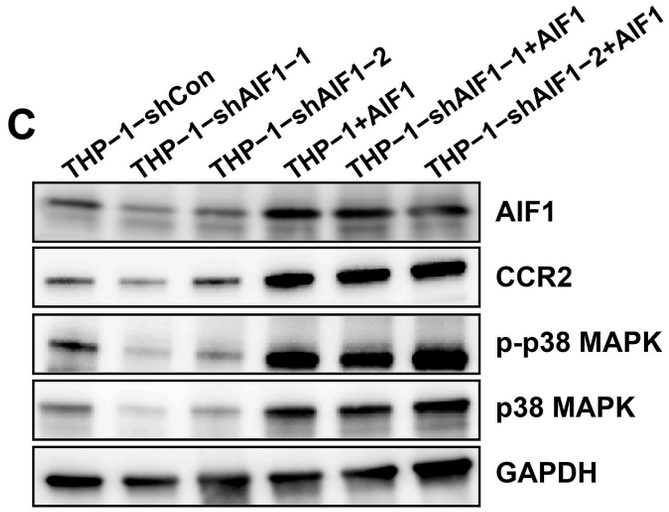
C
THP−1−shCon
THP−1−shAIF1−1
THP−1−shAIF1−2
THP−1+AIF1
THP−1−shAIF1−1+AIF1
THP−1−shAIF1−2+AIF1
AIF1
CCR2
p-p38 MAPK
p38 MAPK
GAPDH

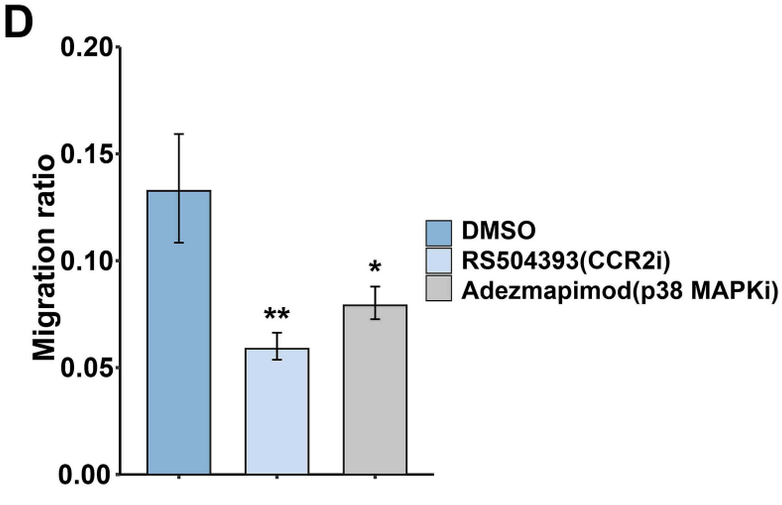
D
Migration ratio
0.20
0.15
0.10
0.05
0.00
**
*
DMSO
RS504393(CCR2i)
Adezmapimod(p38 MAPKi)

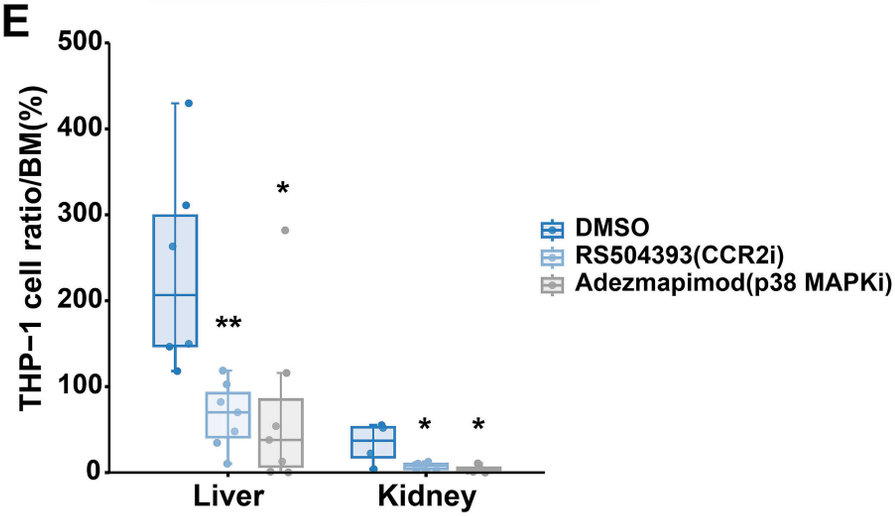
E
THP−1 cell ratio/BM(%)
500
400
300
200
100
0
**
*
*
*
Liver
Kidney
DMSO
RS504393(CCR2i)
Adezmapimod(p38 MAPKi)

Supplementary Figure Legends:

Supplementary Figure S1. AIF1 expression and prognosis in various public cohort.

A. The differences in adhesion and migration characteristics between FAB subtypes M4/M5 and other FAB subtypes by GSEA in TCGA, TARGET, GSE1159 and GSE6891 public cohorts.
B. Overlap of genes associated with cell infiltration, specifically highly expressed in the hematopoietic system, and upregulated in M4/M5 subtypes compared to other AML subtypes across four independent datasets.
C. Predicted interaction relationships among the eight overlapping genes by Signaling Network Integrated Analysis Platform (STRING).
D. Distribution of *AIF1* expression in neutrophil/monocyte and non-neutrophil/monocyte cells from healthy donors or AML patients at diagnosis, along with a ridge plot of the expression of *AIF1* in different cell types from AML patients at diagnosis in scRNA-seq data.
E. The expression of *AIF1* in different AML FAB subtypes, healthy individuals (N= 8) vs CD14 top quartile AML patient blasts (N=70) in the GSE1159.
F. The expression of *AIF1* in different AML FAB subtypes, *AIF1* healthy individuals (N= 19) vs CD14 top quartile AML patient blasts (N=76) in the Beat AML.
G. The expression of *AIF1* in different AML FAB subtypes and risk groups in the GSE14468.
H. Kaplan-Meier curves showing the event-free survival (EFS) and overall survival (OS) of TARGET-AML patients stratified by the median expression of *AIF1*.
I. Kaplan-Meier curves showing the event-free survival (EFS) and overall survival (OS) of TARGET M4&M5 AML patients stratified by the median expression of *AIF1*.
J. Univariate Cox regression analysis was performed to evaluate the prognostic impact of *AIF1* expression on event-free survival (EFS) and overall survival (OS) in three independent cohorts (TCGA, TARGET, and GSE37642). Based on AIF1 expression levels, patients were divided into high- and low-expression groups using the best cutoff determined by the survminer R package. This analysis was applied to the overall cohort as well as to the M1, M2, M4, and M5 FAB subtypes. Hazard ratios (HRs) with 95% confidence intervals (CIs) and p-values were calculated to assess the risk associated with higher *AIF1* expression.

Statistical significance: *p<0.05, **p<0.01, ***p<0.001;
Comparisons: * vs. mean expression level of *AIF1* (Anova test).

Supplementary Figure S2. AIF1 is essential for AMoL growth and infiltration.

Monocytic and non-monocytic cell lines were transduced with scramble control (shCon) and *AIF1* shRNA (sh*AIF1*-1/2) by lentivirus. RNA was extracted 48 hours after sorting,

and *AIF1* expression levels were assessed using real-time quantitative PCR. Relative *AIF1* expression of each sample was normalized to its GAPDH expression and then compared with shCon.

A. Relative *AIF1* expression and growth curves of monocytic cell lines U937 and MV4-11 following *AIF1* knockdown.
B. Relative *AIF1* expression and growth curves of non-monocytic cell lines Kasumi and K562 following *AIF1* knockdown.
C. Left panel: Cell apoptosis of THP-1 cells transduced with shCon or sh*AIF1*, assessed by flow cytometry, stained by Annexin-V and 7AAD. Right panel: Cell cycle change of THP-1, U937 and MV4-11 cells transduced with shCon or sh*AIF1*, assessed by flow cytometry, stained by PI.
D. Migration or invasion assay of U937 or THP-1 cells transduced with shCon, sh*AIF1* and/or *AIF1*. For invasion assay, Transwell inserts were coated with Matrigel. Cells were serum-starved for 20 hours, then seeded into the upper chamber. The lower chamber contained RPMI 1640 medium with 20% FBS. After 5 hours of incubation at 37°C with 5% CO_2, cells infiltrated to the lower chamber were counted to calculate the invasion ratio.
E. Relative *AIF1* expression and migration assay of non-monocytic cell line Kasumi-1 following *AIF1* overexpression. Left panel: Relative *AIF1* expression normalized to its GAPDH expression. Right panel: Migration ratio of Kasumi-1 cells transduced with *AIF1*. Cells migrated to the lower chamber are counted to calculate migration ratio.
F. Adhesion assay of THP-1 and U937 cells transduced with shCon or sh*AIF1* to MS-5 mouse bone marrow stromal cells. Cells were co-cultured for 1h, and washed with medium twice, the rest of cells were quantified to calculate the adhesion ratio of THP-1 to MS-5 cells.
G. Infiltration of *AIF1*-knockdown THP-1 cells (mCherry-positive cells) in the bone marrow, liver, and kidneys of NSG mice after transplantation.

Statistical significance: *p<0.05, **p<0.01, ***p<0.001;
Comparisons: * vs. shCon，# vs. +*AIF1*, $ vs. sh*AIF1*-1, & vs. sh*AIF1*-2 (t-test).

Supplementary Figure S3. *AIF1* knockdown down-regulated expression of CCR2 while *AIF1* overexpression didn't affect CCR2 expression.

A. Pathway enrichment analysis using Metascape for genes that are consistently downregulated/upregulated under all four conditions (2 cell lines, 2 shRNA) and significantly downregulated in at least two conditions (p<0.05).
B. CCR2 expression on the cell surfaces of THP-1 cells (knockdown or overexpress *AIF1*). Right panel: Mean Fluorescence Intensity (MFI) of CCR2 on the surface of THP-1 cells measured by flow cytometry in three independent experiments.

C. Endogenous CCR2 expression in THP-1 cells transduced with shCon or sh*AIF1* and/or *AIF1*. Relative CCR2 expression of each sample was normalized to its GAPDH expression and then compared with shCon.
D. CCR2 expression on the cell surfaces of U937 cells (knockdown or overexpress *AIF1*). Right panel: Mean Fluorescence Intensity (MFI) of CCR2 on the surface of U937 cells measured by flow cytometry in three independent experiments.
E. Endogenous CCR2 expression of U937 cells transduced with shCon or sh*AIF1*.
F. Downregulation of CCR2 in bulk RNA sequencing after sh*AIF1*-1 and sh*AIF1*-2 knockdown compared to the empty control.
G. Expression of CCR2 in different FAB subtypes in the TCGA cohort, showing a strong positive correlation with *AIF1* expression.

Statistical significance: *p<0.05, **p<0.01, ***p<0.001;

Comparisons: * vs. shCon (t-test) or mean expression level of *AIF1* (Anova test), # vs. +*AIF1* (t-test).

Figure_S1

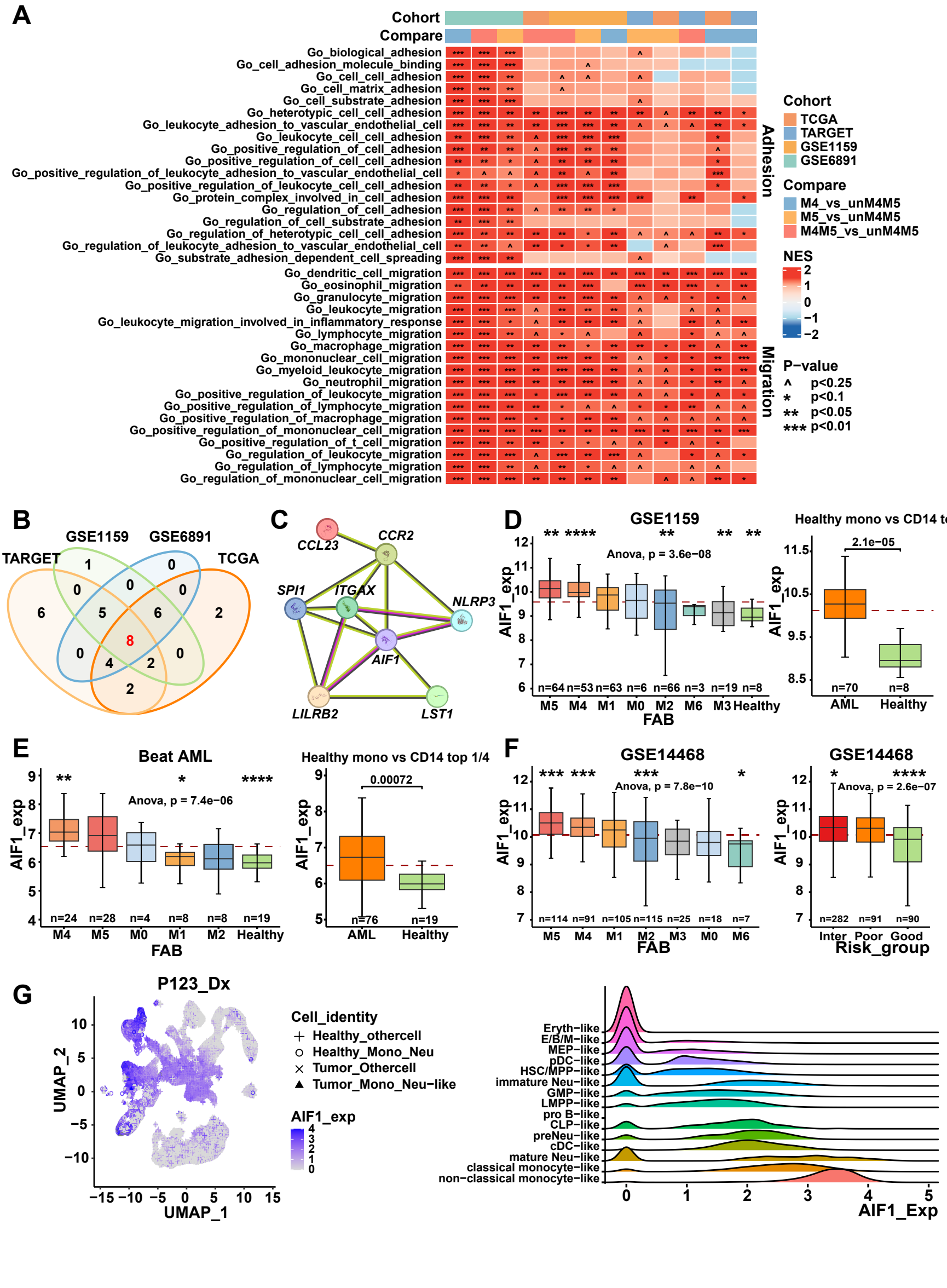
A
Cohort
Compare
Go_biological_adhesion
Go_cell_adhesion_molecule_binding
Go_cell_cell_adhesion
Go_cell_matrix_adhesion
Go_cell_substrate_adhesion
Go_heterotypic_cell_cell_adhesion
Go_leukocyte_adhesion_to_vascular_endothelial_cell
Go_leukocyte_cell_cell_adhesion
Go_positive_regulation_of_cell_adhesion
Go_positive_regulation_of_cell_cell_adhesion
Go_positive_regulation_of_leukocyte_adhesion_to_vascular_endothelial_cell
Go_positive_regulation_of_leukocyte_cell_cell_adhesion
Go_protein_complex_involved_in_cell_adhesion
Go_regulation_of_cell_adhesion
Go_regulation_of_cell_substrate_adhesion
Go_regulation_of_heterotypic_cell_cell_adhesion
Go_regulation_of_leukocyte_adhesion_to_vascular_endothelial_cell
Go_substrate_adhesion_dependent_cell_spreading
Adhesion
Go_dendritic_cell_migration
Go_eosinophil_migration
Go_granulocyte_migration
Go_leukocyte_migration
Go_leukocyte_migration_involved_in_inflammatory_response
Go_lymphocyte_migration
Go_macrophage_migration
Go_mononuclear_cell_migration
Go_myeloid_leukocyte_migration
Go_neutrophil_migration
Go_positive_regulation_of_leukocyte_migration
Go_positive_regulation_of_lymphocyte_migration
Go_positive_regulation_of_macrophage_migration
Go_positive_regulation_of_mononuclear_cell_migration
Go_positive_regulation_of_t_cell_migration
Go_regulation_of_leukocyte_migration
Go_regulation_of_lymphocyte_migration
Go_regulation_of_mononuclear_cell_migration
Migration
Cohort
TCGA
TARGET
GSE1159
GSE6891
Compare
M4_vs_unM4M5
M5_vs_unM4M5
M4M5_vs_unM4M5
NES
2
1
0
−1
−2
P−value
^ p<0.25
* p<0.1
** p<0.05
*** p<0.01
B
GSE1159
GSE6891
TARGET
TCGA
C
CCL23
CCR2
SPI1
ITGAX
NLRP3
AIF1
LILRB2
LST1
D
GSE1159
Anova, p = 3.6e−08
AIF1_exp
n=64 n=53 n=63 n=6 n=66 n=3 n=19 n=8
M5 M4 M1 M0 M2 M6 M3 Healthy
FAB
Healthy mono vs CD14 top 1/4
2.1e−05
n=70 n=8
AML Healthy
E
Beat AML
Anova, p = 7.4e−06
n=24 n=28 n=4 n=8 n=8 n=19
M4 M5 M0 M1 M2 Healthy
FAB
Healthy mono vs CD14 top 1/4
0.00072
n=76 n=19
AML Healthy
F
GSE14468
Anova, p = 7.8e−10
n=114 n=91 n=105 n=115 n=25 n=18 n=7
M5 M4 M1 M2 M3 M0 M6
FAB
GSE14468
Anova, p = 2.6e−07
n=282 n=91 n=90
Inter Poor Good
Risk_group
G
P123_Dx
UMAP_1
UMAP_2
Cell_identity
Healthy_othercell
Healthy_Mono_Neu
Tumor_Othercell
Tumor_Mono_Neu−like
AIF1_exp
Eryth−like
E/B/M−like
MEP−like
pDC−like
HSC/MPP−like
immature Neu−like
GMP−like
LMPP−like
pro B−like
CLP−like
preNeu−like
cDC−like
mature Neu−like
classical monocyte−like
non−classical monocyte−like
AIF1_Exp

H

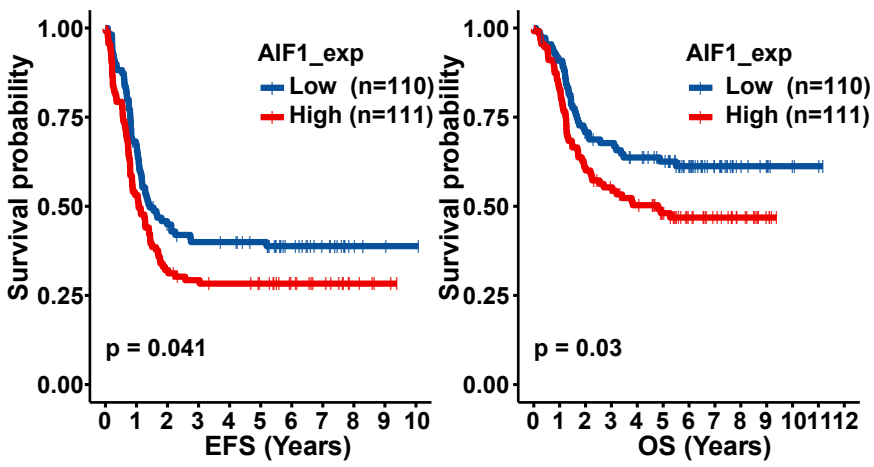

I

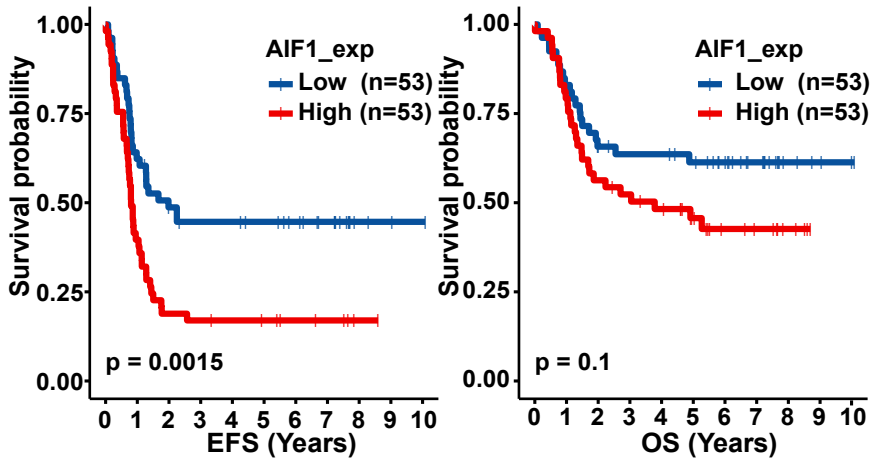

J

	Whole cohort					
	EFS			OS		
	HR	P_value	95CI	HR	P_value	95CI
GSE37642	--	--	--	1.316	0.019	[1.047,1.654]
Target	1.671	0.002	[1.205,2.315]	1.699	0.009	[1.14,2.531]
TCGA	1.665	0.008	[1.14,2.432]	1.934	0.002	[1.281,2.921]

	M1					
	EFS			OS		
	HR	P_value	95CI	HR	P_value	95CI
GSE37642	--	--	--	2.093	0.005	[1.255,3.49]
Target	1.852	0.171	[0.766,4.476]	5.246	0.013	[1.416,19.436]
TCGA	0.844	0.763	[0.28,2.543]	0.629	0.465	[0.182,2.178]

	M2					
	EFS			OS		
	HR	P_value	95CI	HR	P_value	95CI
GSE37642	--	--	--	1.717	0.02	[1.09,2.706]
Target	1.844	0.17	[0.77,4.417]	2.785	0.096	[0.835,9.293]
TCGA	2.801	0.015	[1.225,6.405]	2.931	0.023	[1.158,7.418]

	M4					
	EFS			OS		
	HR	P_value	95CI	HR	P_value	95CI
GSE37642	--	--	--	0.858	0.688	[0.406,1.813]
Target	2.218	0.015	[1.168,4.211]	2.767	0.017	[1.195,6.403]
TCGA	0.883	0.805	[0.328,2.375]	1.321	0.592	[0.477,3.659]

	M5					
	EFS			OS		
	HR	P_value	95CI	HR	P_value	95CI
GSE37642	--	--	--	0.443	0.128	[0.155,1.264]
Target	2.204	0.08	[0.911,5.332]	1.671	0.303	[0.629,4.44]
TCGA	0.42	0.186	[0.116,1.52]	0.395	0.155	[0.11,1.421]

Figure_S2

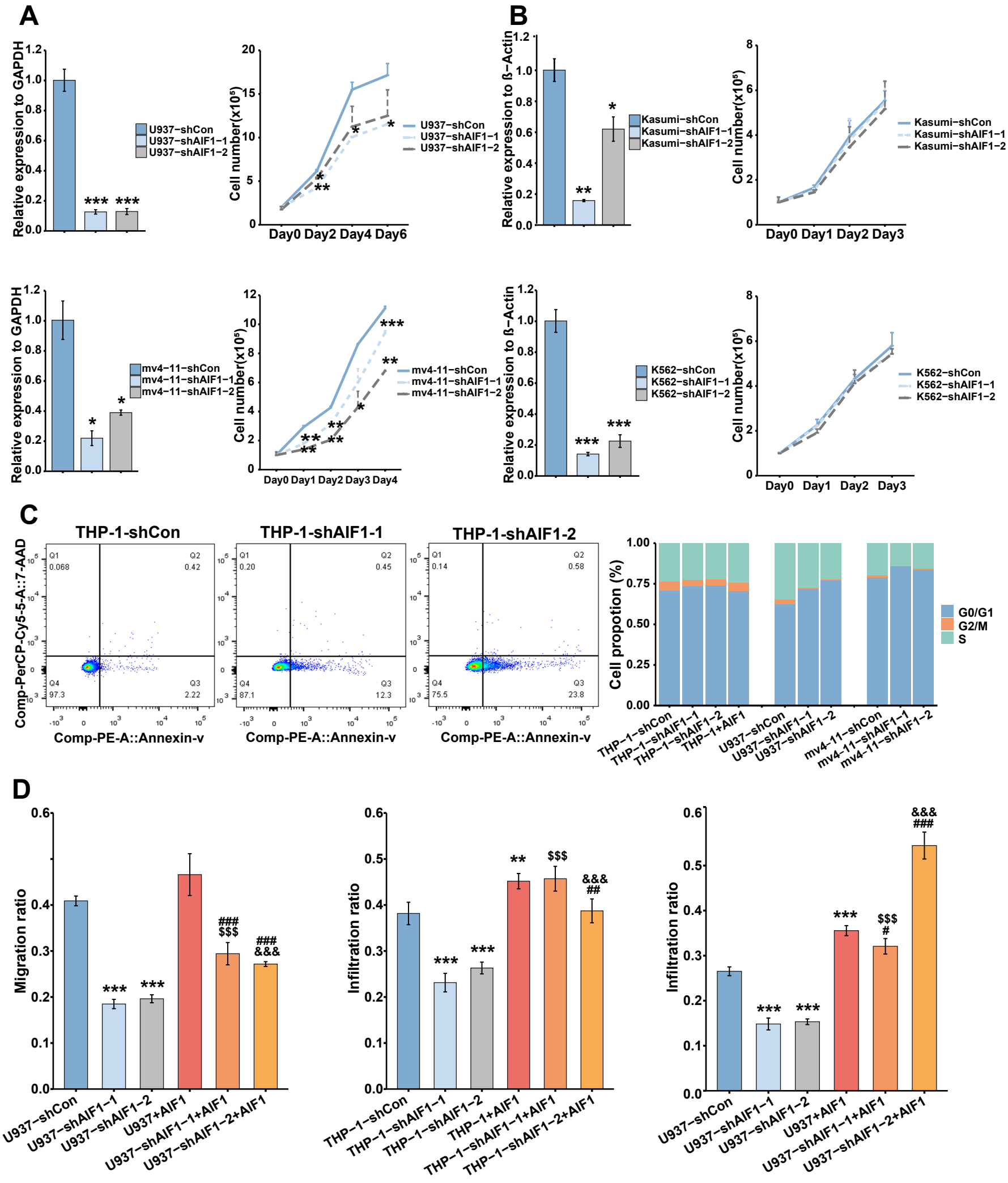
A
Relative expression to GAPDH
U937−shCon
U937−shAIF1−1
U937−shAIF1−2
Cell number(x10⁵)
Day0 Day2 Day4 Day6
B
Relative expression to ß−Actin
Kasumi−shCon
Kasumi−shAIF1−1
Kasumi−shAIF1−2
Day0 Day1 Day2 Day3
mv4−11−shCon
mv4−11−shAIF1−1
mv4−11−shAIF1−2
Day0 Day1 Day2 Day3 Day4
K562−shCon
K562−shAIF1−1
K562−shAIF1−2
C
THP-1-shCon
THP-1-shAIF1-1
THP-1-shAIF1-2
Comp-PerCP-Cy5-5-A::7-AAD
Comp-PE-A::Annexin-v
Q1 0.068
Q2 0.42
Q4 97.3
Q3 2.22
Q1 0.20
Q2 0.45
Q4 87.1
Q3 12.3
Q1 0.14
Q2 0.58
Q4 75.5
Q3 23.8
Cell propotion (%)
G0/G1
G2/M
S
THP−1−shCon
THP−1−shAIF1−1
THP−1−shAIF1−2
THP−1+AIF1
U937−shCon
U937−shAIF1−1
U937−shAIF1−2
mv4−11−shCon
mv4−11−shAIF1−1
mv4−11−shAIF1−2
D
Migration ratio
U937−shCon
U937−shAIF1−1
U937−shAIF1−2
U937+AIF1
U937−shAIF1−1+AIF1
U937−shAIF1−2+AIF1
Infiltration ratio
THP−1−shCon
THP−1−shAIF1−1
THP−1−shAIF1−2
THP−1+AIF1
THP−1−shAIF1−1+AIF1
THP−1−shAIF1−2+AIF1

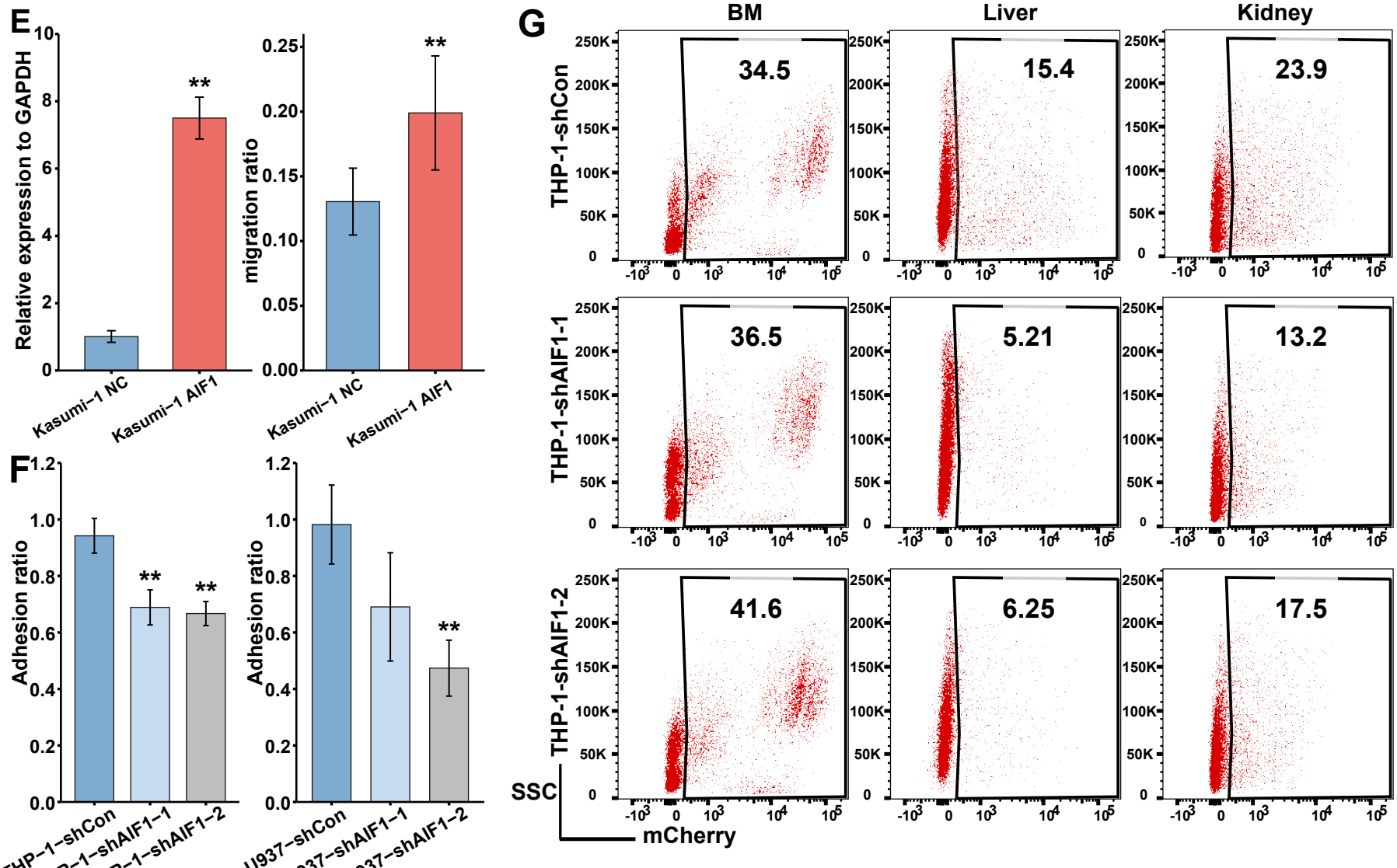
E
Relative expression to GAPDH
Kasumi−1 NC
Kasumi−1 AIF1
migration ratio
Kasumi−1 NC
Kasumi−1 AIF1
F
Adhesion ratio
THP−1−shCon
THP−1−shAIF1−1
THP−1−shAIF1−2
Adhesion ratio
U937−shCon
U937−shAIF1−1
U937−shAIF1−2
G
BM
Liver
Kidney
THP-1-shCon
THP-1-shAIF1-1
THP-1-shAIF1-2
34.5
15.4
23.9
36.5
5.21
13.2
41.6
6.25
17.5
SSC
mCherry

Figure_S3

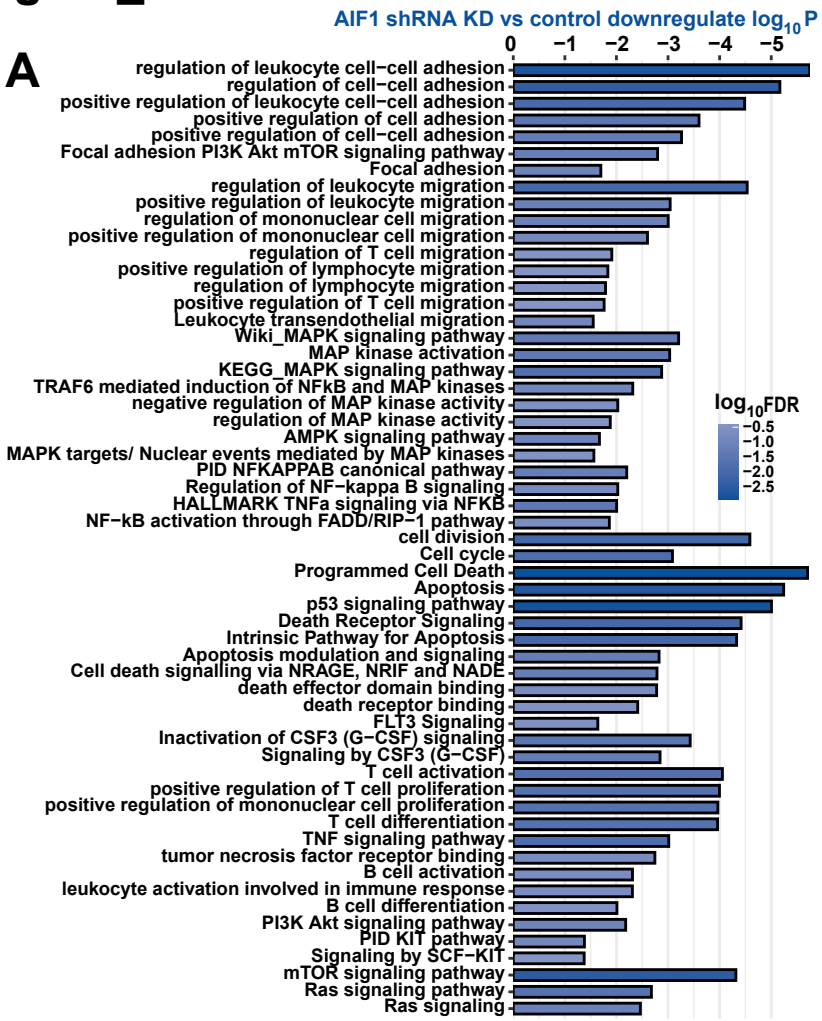
A
AIF1 shRNA KD vs control downregulate log10 P
0 −1 −2 −3 −4 −5
regulation of leukocyte cell−cell adhesion
regulation of cell−cell adhesion
positive regulation of leukocyte cell−cell adhesion
positive regulation of cell adhesion
positive regulation of cell−cell adhesion
Focal adhesion PI3K Akt mTOR signaling pathway
Focal adhesion
regulation of leukocyte migration
positive regulation of leukocyte migration
regulation of mononuclear cell migration
positive regulation of mononuclear cell migration
regulation of T cell migration
positive regulation of lymphocyte migration
regulation of lymphocyte migration
positive regulation of T cell migration
Leukocyte transendothelial migration
Wiki_MAPK signaling pathway
MAP kinase activation
KEGG_MAPK signaling pathway
TRAF6 mediated induction of NFkB and MAP kinases
negative regulation of MAP kinase activity
regulation of MAP kinase activity
AMPK signaling pathway
MAPK targets/ Nuclear events mediated by MAP kinases
PID NFKAPPAB canonical pathway
Regulation of NF−kappa B signaling
HALLMARK TNFa signaling via NFKB
NF−kB activation through FADD/RIP−1 pathway
cell division
Cell cycle
Programmed Cell Death
Apoptosis
p53 signaling pathway
Death Receptor Signaling
Intrinsic Pathway for Apoptosis
Apoptosis modulation and signaling
Cell death signalling via NRAGE, NRIF and NADE
death effector domain binding
death receptor binding
FLT3 Signaling
Inactivation of CSF3 (G−CSF) signaling
Signaling by CSF3 (G−CSF)
T cell activation
positive regulation of T cell proliferation
positive regulation of mononuclear cell proliferation
T cell differentiation
TNF signaling pathway
tumor necrosis factor receptor binding
B cell activation
leukocyte activation involved in immune response
B cell differentiation
PI3K Akt signaling pathway
PID KIT pathway
Signaling by SCF−KIT
mTOR signaling pathway
Ras signaling pathway
Ras signaling
log10FDR
−0.5
−1.0
−1.5
−2.0
−2.5
AIF1 shRNA KD vs control upregulate log10 P
0 −2 −4 −6 −8 −10
intracellular protein transport
protein localization to endoplasmic reticulum
establishment of protein localization to membrane
protein localization to membrane
protein localization to organelle
protein targeting to membrane
establishment of protein localization to endoplasmic reticulum
protein targeting to ER
establishment of protein localization to organelle
post−translational protein targeting to ERM
post−translational protein targeting to membrane, translocation
cotranslational protein targeting to membrane
SRP−dependent cotranslational protein targeting to membrane
intracellular protein transmembrane transport
mRNA Splicing
mRNA Splicing − Major Pathway
Processing of Capped Intron−Containing Pre−mRNA
RNA splicing, via transesterification reactions
mRNA splicing, via spliceosome
mRNA processing
mRNA metabolic process
Unfolded Protein Response (UPR)
response to unfolded protein
proteasomal protein catabolic process
response to topologically incorrect protein
proteolysis involved in protein catabolic process
cellular response to unfolded protein
cellular response to topologically incorrect protein
endoplasmic reticulum unfolded protein response
Adaptive Immune System
Neutrophil degranulation
Antigen processing−Cross presentation
Class I MHC mediated antigen processing & presentation
Folding, assembly and peptide loading of class I MHC
Cytokine Signaling in Immune system
antigen processing and presentation of peptide antigen
MHC class II antigen presentation
antigen processing and presentation of exogenous antigen
cellular respiration
oxidative phosphorylation
electron transport chain
energy derivation by oxidation of organic compounds
aerobic electron transport chain
proton motive force−driven mitochondrial ATP synthesis
ATP synthesis coupled electron transport
mitochondrial ATP synthesis coupled electron transport
mitochondrial electron transport, NADH to ubiquinone
proton motive force−driven ATP synthesis
NADH dehydrogenase complex assembly
mitochondrial respiratory chain complex I assembly
log10FDR
−2
−4
−6
B
THP-1-AIF1
THP-1-Con
THP-1-shAIF1-2
THP-1-shAIF1-1
THP-1-shCon
-10^3 0 10^3 10^4 10^5
Comp-APC-A::CCR2
Mean MFI of APC
0.17
0.103
0.07
THP1−1−shCon
THP−1−shAIF1−1
THP−1−shAIF1−2
THP−1+Con
THP−1+AIF1
C
Relative expression to GAPDH
**
**
###
##
THP−1−shCon
THP−1−shAIF1−1
THP−1−shAIF1−2
THP−1+AIF1
THP−1−shAIF1−1+AIF1
THP−1−shAIF1−2+AIF1
D
U937-AIF1
U937-Con
U937-shAIF1-2
U937-shAIF1-1
U937-shCon
-10^3 0 10^3 10^4 10^5
Comp-APC-A::CCR2
Mean MFI of APC
0.126
0.131
0.186
U937−shCon
U937−shAIF1−1
U937−shAIF1−2
U937+Con
U937+AIF1
E
Relative expression to GAPDH
***
**
U937−shCon
U937−shAIF1−1
U937−shAIF1−2
F
CCR2_exp log (TPM+1)
0.01
0.004
THP−1−shCon
THP−1−shAIF1−1
THP−1−shAIF1−2
0.18
0.18
U937−shCon
U937−shAIF1−1
U937−shAIF1−2
G
TCGA
*
****
****
Anova, p = 3.2e−10
CCR2_exp
n=15 n=29 n=35 n=38 n=15 n=2 n=14
M5 M4 M1 M2 M0 M6 M3
FAB
TCGA
R=0.27p=8e−04
CCR2_exp
AIF1_exp